Supporting Information

The different nature of the interactions between anions and $HAT(CN)_6$: from reversible anion-π complexes to irreversible electron transfer processes ($HAT(CN)_6$ = 1,4,5,8,9,12-hexaazatriphenylene)

Gemma Aragay,[a] Antonio Frontera,[c] Vega Lloveras[d], José Vidal-Gancedo[d] and Pablo Ballester[a,b*]

[a] Institute of Chemical Research of Catalonia (ICIQ), Avgda. Països Catalans 16, 43007 Tarragona, Spain

[b] Catalan Institution for Research and Advanced Studies (ICREA), Passeig Lluís Companys, 23, 08018 Barcelona, Spain

[c] Departament de Química, Universitat de les Illes Balears (UIB), 07122 Palma de Mallorca, Spain

[d] ICMAB-CSIC, Campus de Bellaterra, 08193 Bellaterra, Barcelona, and CIBER-BBN, Barcelona, Spain.

Contents

1. General Methods and Instrumentation

Starting materials and reagents were purchased from Sigma Aldrich and used as received. All reactions were performed under N_2 atmosphere. Anhydrous solvents were obtained from a solvent purification system SPS-400-6 from Innovative Technologies, Inc. All solvents were of HPLC grade quality, commercially obtained and used without further purification.

^{1}H , $^{13}C\{^{1}H\}$ and ^{19}F NMR spectra were recorded on a Bruker Avance II 400 Ultrashield NMR spectrometer. ^{19}F-^{19}F EXSY and variable temperature experiments were performed on a Bruker Avance 500 (500.1 MHz for ^{1}H NMR) Ultrashield spectrometer. CD_3CN from Sigma Aldrich was used for NMR studies. Chemical shifts are given in ppm, relative to TMS. The ^{19}F NMR chemical shifts were measured using CCl_3F in $CDCl_3$ as reference.

The ESR spectra were obtained using a Bruker ELEXYS E500 X band spectrometer equipped with a field-frequency (F/F) lock accessory and built in NMR Gaussmeter. A rectangular TE102 cavity was used for the measurements. The signal to noise ratio of spectra was increased by accumulation of scans using the F/F lock accessory to guarantee large field reproducibility. Precautions to avoid undesirable spectral distortions and line broadenings, such as those arising from microwave power saturation and magnetic field over modulation, were also taken into account. To avoid dipolar line broadening from dissolved oxygen, solutions were always carefully degassed with pure Argon. To control the temperature a Bruker Variable Temperature Unit was used.

The conductometric titrations were performed using a Mettler-Toledo conductimeter, with a 84µS/cm sensor previously calibrated with a 0.00056 M KCl solution.

Cyclic voltammetry (CV) experiments were performed on a BASi Epsilon potentiostat connected to a C3 standard electrochemical cell, consisting of a Pt gauche working electrode, Pt-wire counter electrode, and a Ag/AgCl reference electrode. UV-Vis measurements were performed in a UV-2401 PC from Shimadzu Corporation.

2. Experimental procedures

$HAT(CN)_6$ was obtained following the procedure described in the literature. [1] $^{13}C\{^1H\}$ NMR ((CD_3CN)) δ 142.0 (C_B), 135.8 (C_A), 114.6 (C_C). FT-IR (ATR): ν(CN) 2242 cm^{-1}.

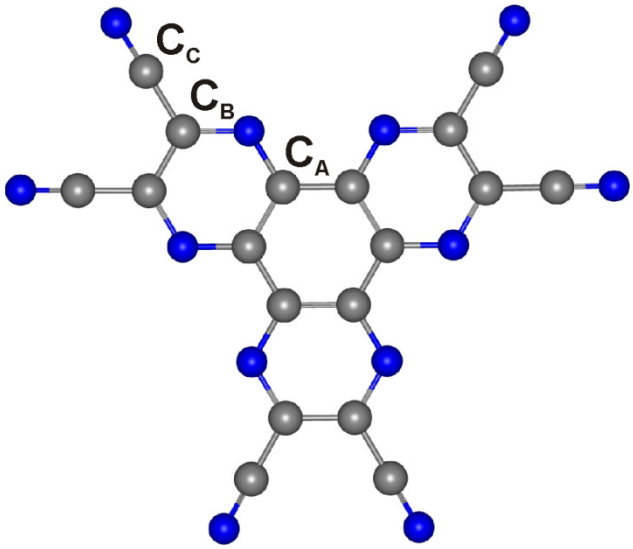

Figure S1. Molecular structure of $HAT(CN)_6$ (**1**) and carbon assignment.

meso-tetra *p*-nitrophenyl-tetramethyl calix[4]pyrrole was obtained following the procedure described in the literature.[2]

3. DFT calculations

The HOMO-LUMO energy levels of different species of **1**, and anions used in the present work were calculated using DFT with the Gaussian 09 program.[3] The BP86 functional was used, along with def2-TZVP basis set considering CH_3CN solvation by means of the Polarizable Continuum Model (PCM). The consideration solvation of effects in the calculation of the energy levels is important since the HOMO energy values of the anions are strongly influenced. A strong disagreement between theory and experiment is observed if gas-phase values are considered.

The optimization of the complex between $[HAT(CN)_6]^-$ and either F^- or ^-OH was performed without imposing symmetry constrains at the BP86-D3/def2-TZVPD level of

theory using the program TURBOMOLE version 6.4.[4] The interaction energies were computed taking into account solvent effects by means of the Polarizable Continuum Model (PCM) using the integral equation formalism variant (IEFPCM).[5] The geometry of both complexes belongs to the C1 point group and they are stationary points. The geometries are shown in Figure S2. The equilibrium distances (measured from the anion to the ring centroid) are shorter compared to standard anion–π interactions (> 3 Å), indicating some degree of covalent bonding in the interaction.

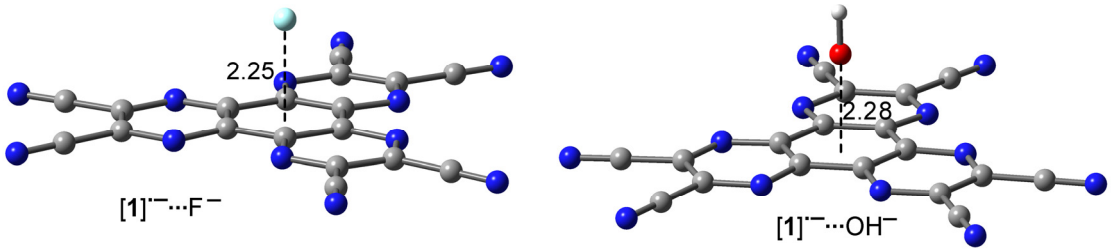

Figure S2. BP86-D3/def2-TZVP optimized geometries of the complexes between $[\mathbf{1}]^{\bullet-}$ and F^- and ^-OH anions. Distances in Å.

Cartesian coordinates of the complexes:

[**1**]$^{\cdot-}\cdots F^{-}$

C	0.7053656	3.5395772	0.1154871
C	0.7106433	1.2532453	0.0567170
C	-0.7113396	1.2522898	0.0457473
C	-0.7063687	3.5394117	0.0905564
C	1.4401157	-0.0099062	0.0446489
C	-1.4401128	-0.0113266	0.0578478
C	-0.7280735	-1.2421303	0.0484157
C	0.7297598	-1.2418996	0.0607561
C	-2.7116304	-2.3810586	0.0907255
C	-3.4179443	-1.1586572	0.1129017
C	3.4186937	-1.1581091	0.0861562
C	2.7127987	-2.3804521	0.1188274
N	1.3645349	-2.4325032	0.1183940
N	2.7892450	0.0360765	0.0698267
N	1.4244109	2.3978417	0.1104275
N	-1.4254871	2.3976977	0.0753810
N	-2.7879829	0.0353422	0.1093397
N	-1.3635978	-2.4337659	0.0787518
C	-3.4210531	-3.6279163	0.1007704
C	-4.8509994	-1.1486261	0.1644358
C	-1.4328512	4.7760693	0.1021577
C	1.4315067	4.7751803	0.1715056
C	3.4204023	-3.6267819	0.1759829
C	4.8525887	-1.1491514	0.0917035
N	4.0128292	-4.6309989	0.2302139
N	6.0197153	-1.1622154	0.1042776
N	2.0065278	5.7894626	0.2257927
N	-2.0075111	5.7918707	0.1197063
N	-6.0171940	-1.1592869	0.2148018
N	-4.0169859	-4.6314029	0.1164687
F	-0.0000060	0.0021238	-2.1971778

[**1**]$^{-}\cdots^{-}$OH

C	-3.5412885	0.7062938	0.1697999
C	-1.2532586	0.7120526	0.1037932
C	-1.2531274	-0.7119507	0.1037610
C	-3.5413529	-0.7062076	0.1698069
C	0.0097091	1.4424676	0.1040839
C	0.0096461	-1.4422964	0.1041198
C	1.2425636	-0.7288484	0.1053928
C	1.2423206	0.7286949	0.1053917
C	2.3820702	-2.7133950	0.1704220
C	1.1591707	-3.4205999	0.1698495
C	1.1591690	3.4205860	0.1698370
C	2.3819483	2.7133244	0.1704331
N	2.4338733	1.3651608	0.1580445
N	-0.0352147	2.7914449	0.1561292
N	-2.3997801	1.4253417	0.1562221
N	-2.3997253	-1.4252945	0.1561927
N	-0.0352081	-2.7913952	0.1561683
N	2.4340689	-1.3651862	0.1579898
C	3.6298669	-3.4193442	0.2099127
C	1.1477090	-4.8536109	0.2098382
C	-4.7761823	-1.4342018	0.2100981
C	-4.7763118	1.4341624	0.2100983
C	3.6298743	3.4191864	0.2099180
C	1.1476993	4.8537027	0.2098272
N	4.6369710	4.0083371	0.2490621
N	1.1533310	6.0205471	0.2499368
N	-5.7891530	2.0137302	0.2501138
N	-5.7890835	-2.0137471	0.2501146
N	1.1533310	-6.0205366	0.2499375
N	4.6370610	-4.0084210	0.2490672
O	0.0010253	-0.0000722	-2.1844998
H	-0.0017222	0.0000753	-3.1608619

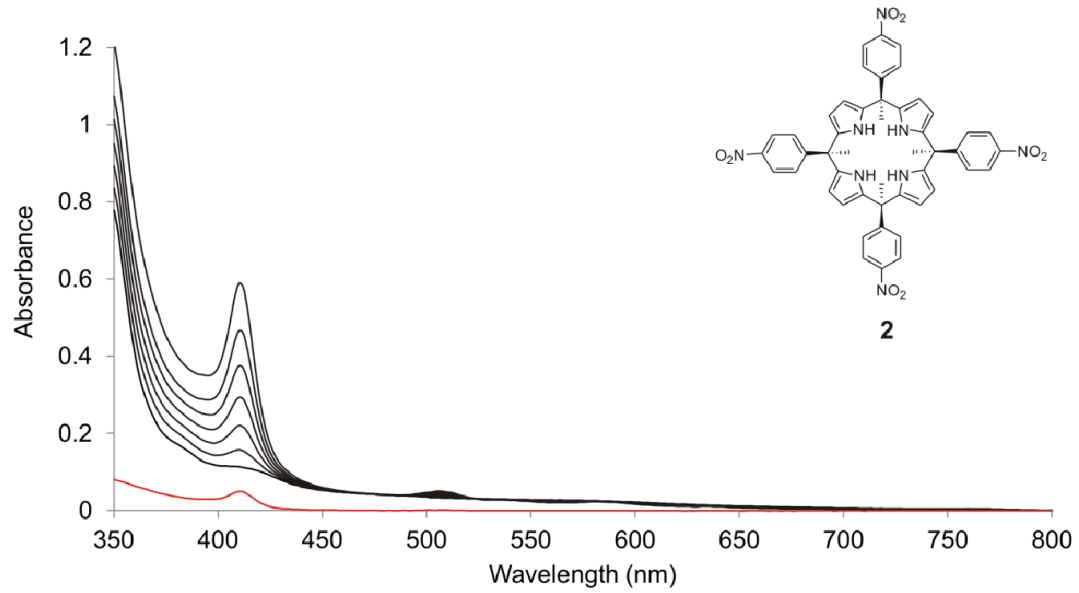

Figure S3. UV-Vis spectra of the titration of **1** (0.11 mM) in CH_3CN solution with an equimolar solution of TBAF and meso-tetra *p*-nitrophenyl-tetramethyl calix[4]pyrrole (**2**) ([2]=[TBAF]=1.1 mM. Black solid lines: **1** + 0, 0.4, 0.6, 0.8, 1.0, 1.5, and 2 equiv of **2** + TBAF added). Inset: Structure of meso-tetra *p*-nitrophenyl-tetramethyl calix[4]pyrrole (**2**). Up to 2 equiv of the $F^-\subset$**2** complex were added. (Red solid line: UV-Vis spectrum of an equimolar CH_3CN solution of the titrant **2** + TBAF at a concentration of [2]=[TBAF] = 0.01 mM.

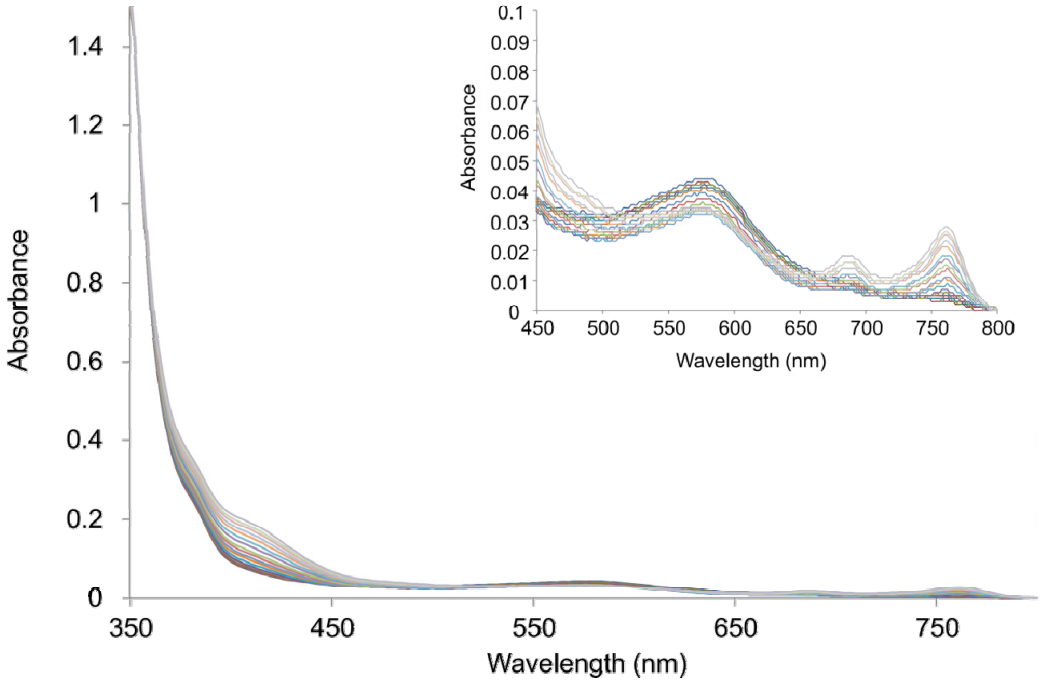

Figure S4. UV-Vis spectra of the titration of **1** in CH_3CN solution (0.14 mM) with TBACl (up to 60 equiv of TBACl were added). Inset: Expansion of the region of the spectra from 450 to 800 nm.

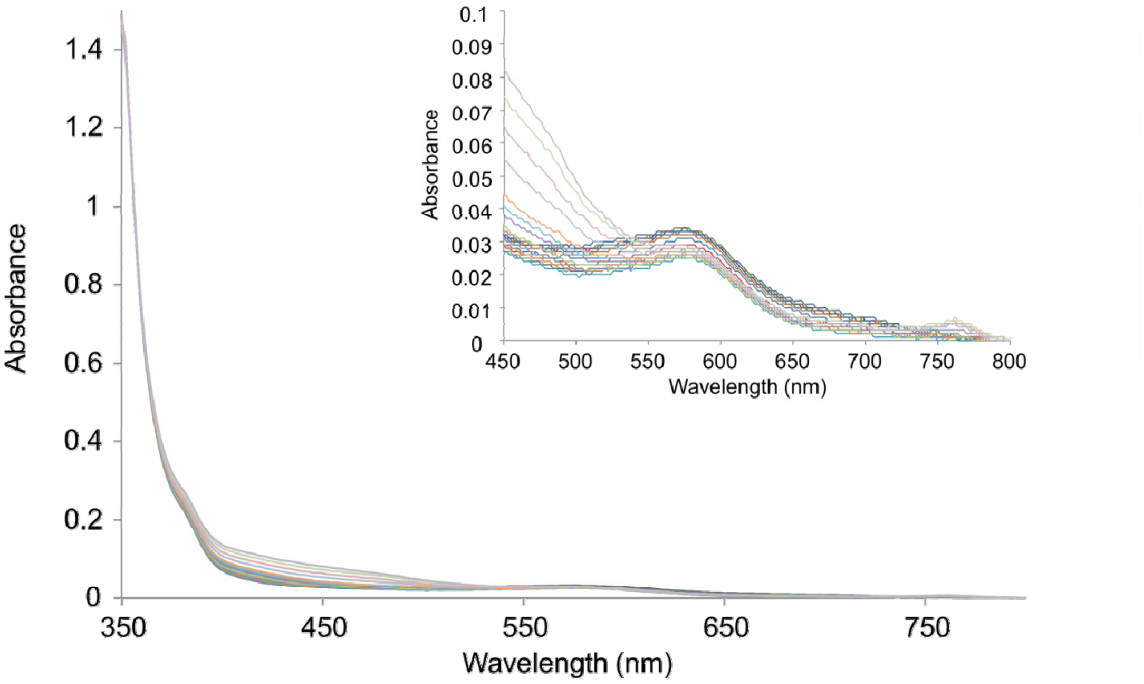

Figure S5. UV-Vis spectra of the titration of **1** in CH_3CN solution (0.14 mM) with TBABr (up to 60 equiv of TBABr were added). Inset: Expansion of the region of the spectra from 450 to 800 nm.

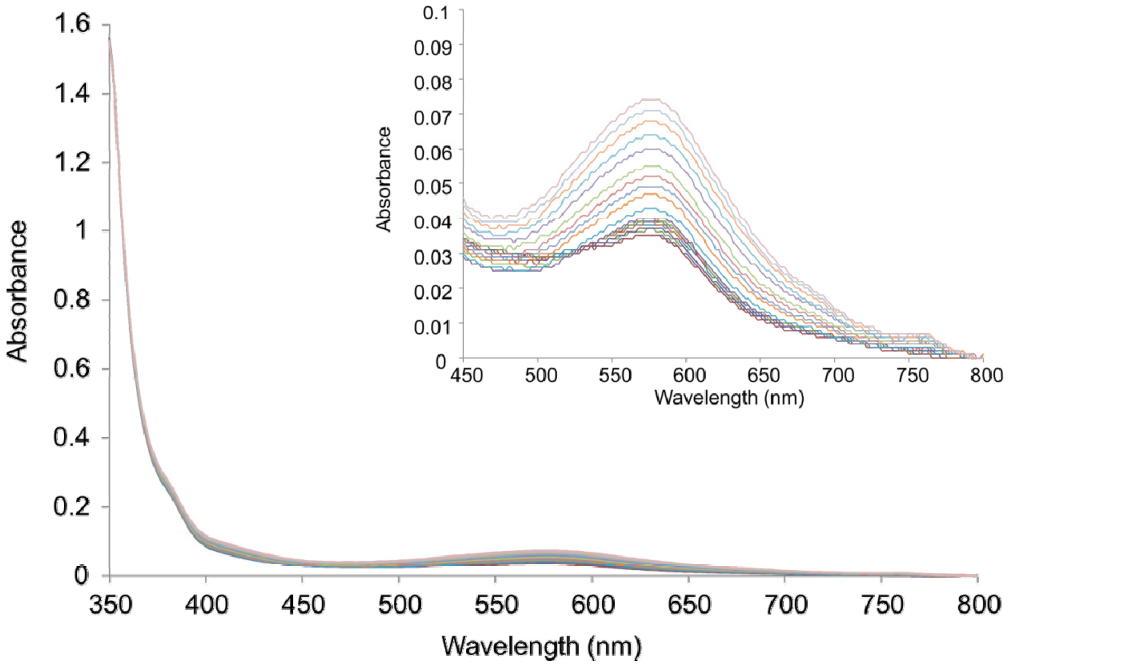

Figure S6. UV-Vis spectra of the titration of **1** in CH_3CN solution (0.14 mM) with TBAI (up to 70 equiv of TBAI were added). Inset: Expansion of the region of the spectra from 450 to 800 nm.

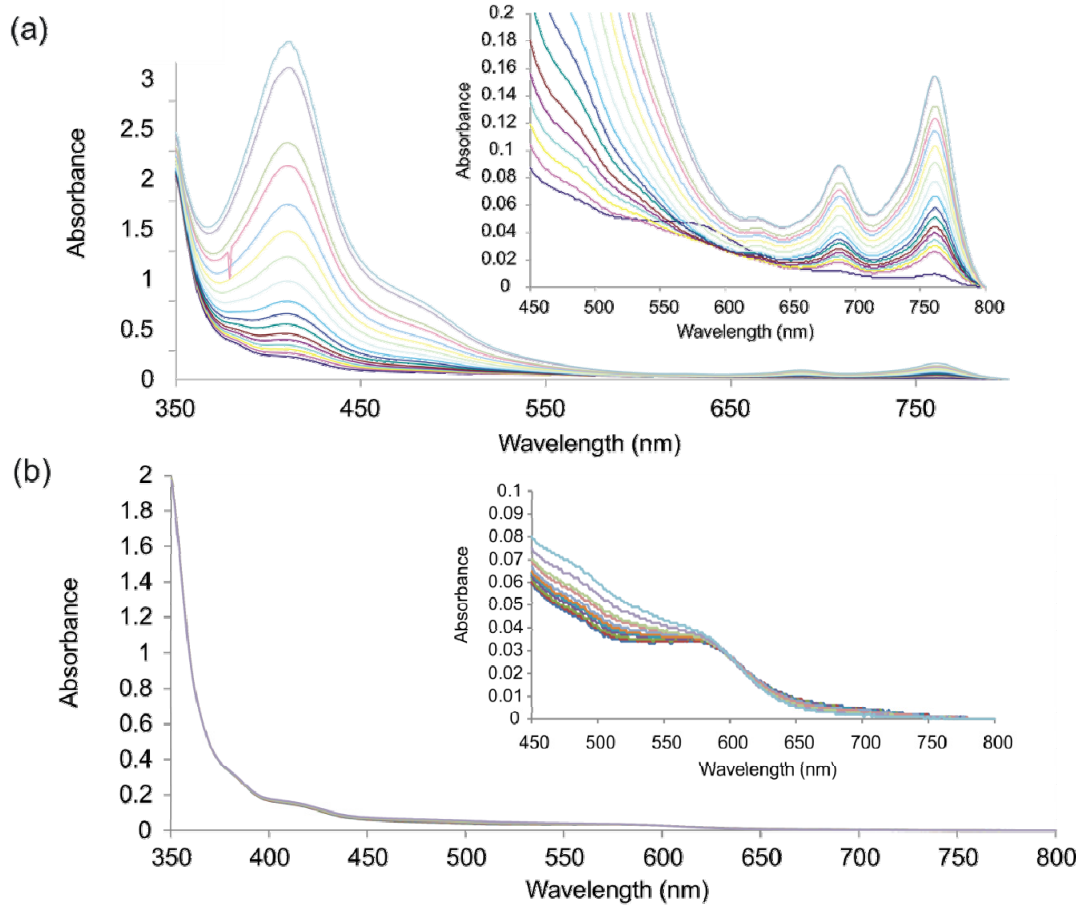

Figure S7. UV-Vis spectra of the titration of **1** in CH_3CN solution (0.14 mM) with TBA(OCN) (a) and TBA(SCN) (b) (up to 30 and 40 equiv of TBA(OCN) and TBA(SCN) were added, respectively). Inset: Expansion of the region of the spectra from 450 to 800 nm.

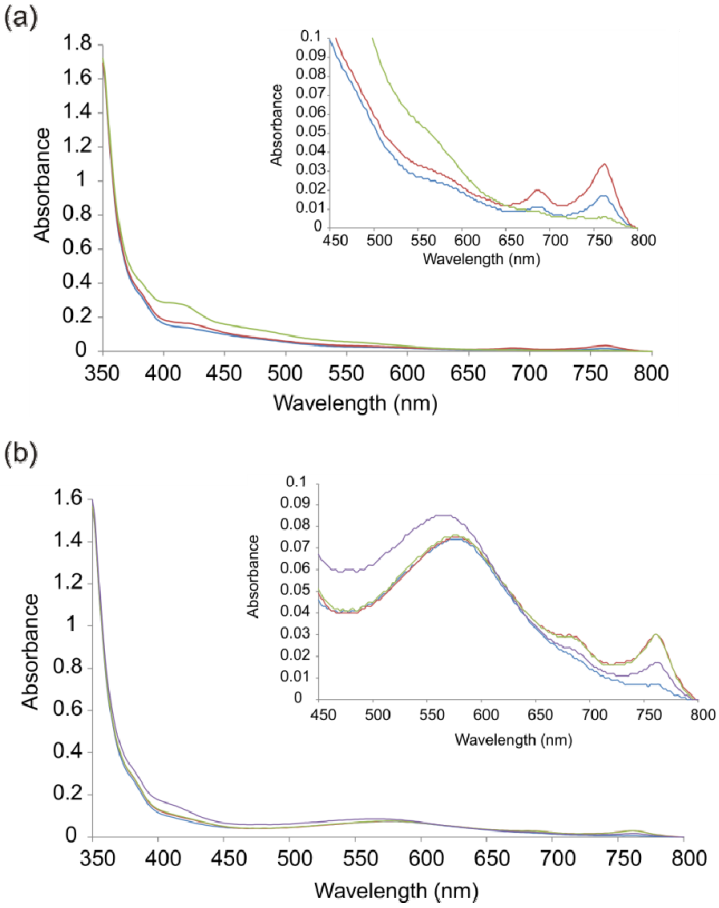

Figure S8. Photoinduced electron transfer study (the three spectra were acquired during 5 minutes of irradiation at 365 nm) of **1** in CH_3CN (0.14 mM) with TBABr (a) and TBAI (b) (60 equiv of TBABr or TBAI were added). Inset: Expansion of the region of the spectra from 450 to 800 nm.

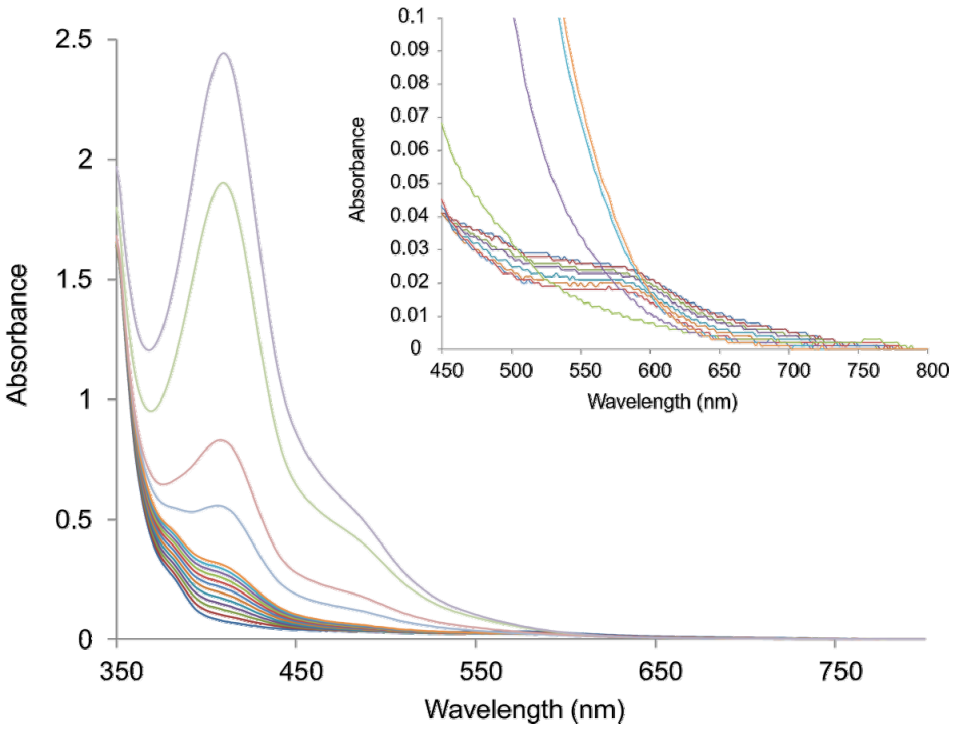

Figure S9. Photoinduced electron transfer study (the spectra were acquired at different intervals during a total time of 5 minutes of irradiation at 365 nm) of **1** in CH_3CN (0.14 mM) with TBACl (60 equiv of TBACl were added). Inset: Expansion of the region of the spectra from 450 to 800 nm.

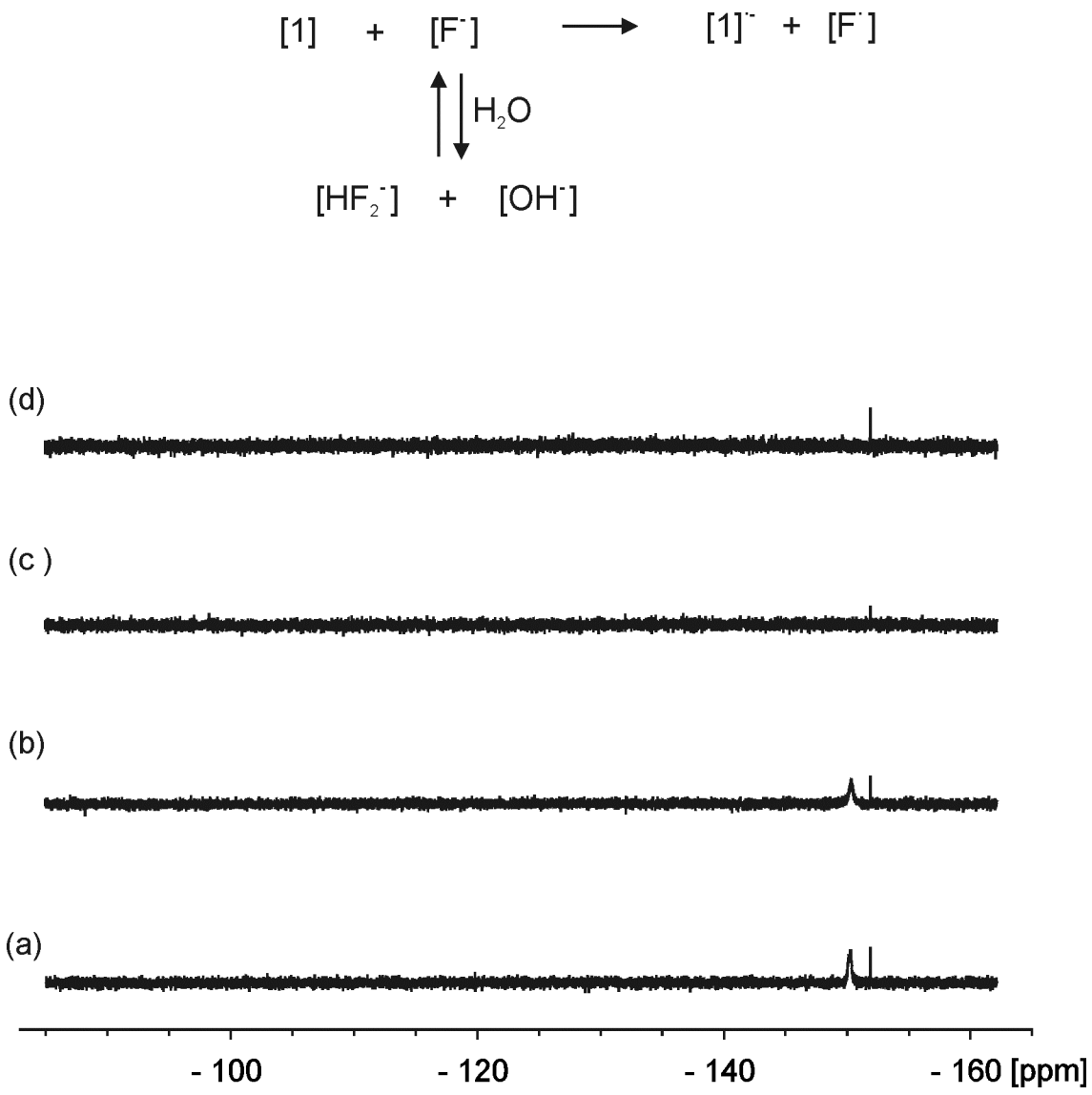

Figure S10. ^{19}F NMR titration (CD_3CN, 298 K) of TBAF·$3H_2O$ (1 mM) with 0 (a), 0.25 (b), 1.2 (c), 1.5 equiv (d) of **1**.

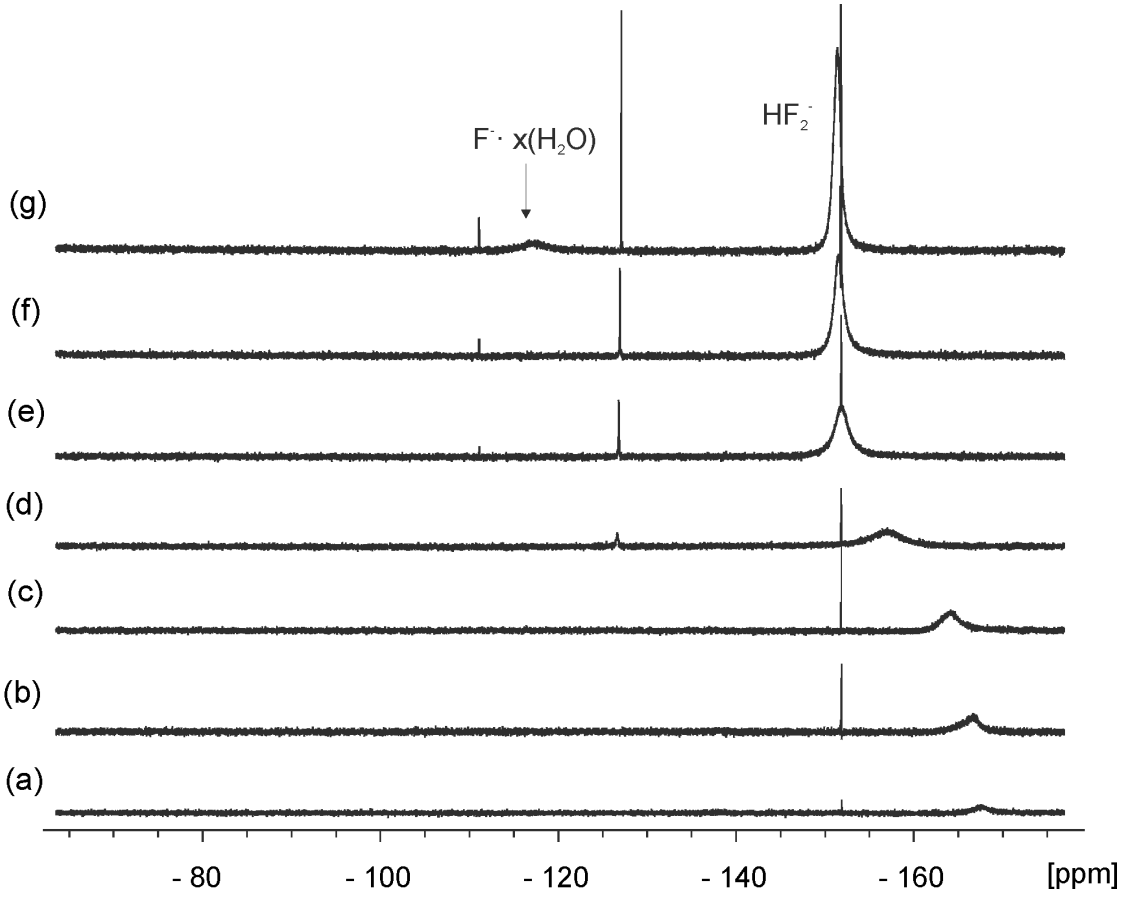

Figure S11. ^{19}F NMR titration (CD_3CN, 298 K) of **[1]** (7 mM) with 0.5 (a), 1.0 (b), 2.0 (c), 3.0 (d), 5.0 (e), 7.0 (f), 10.0 equiv (g) of $TBAF \cdot 3H_2O$.

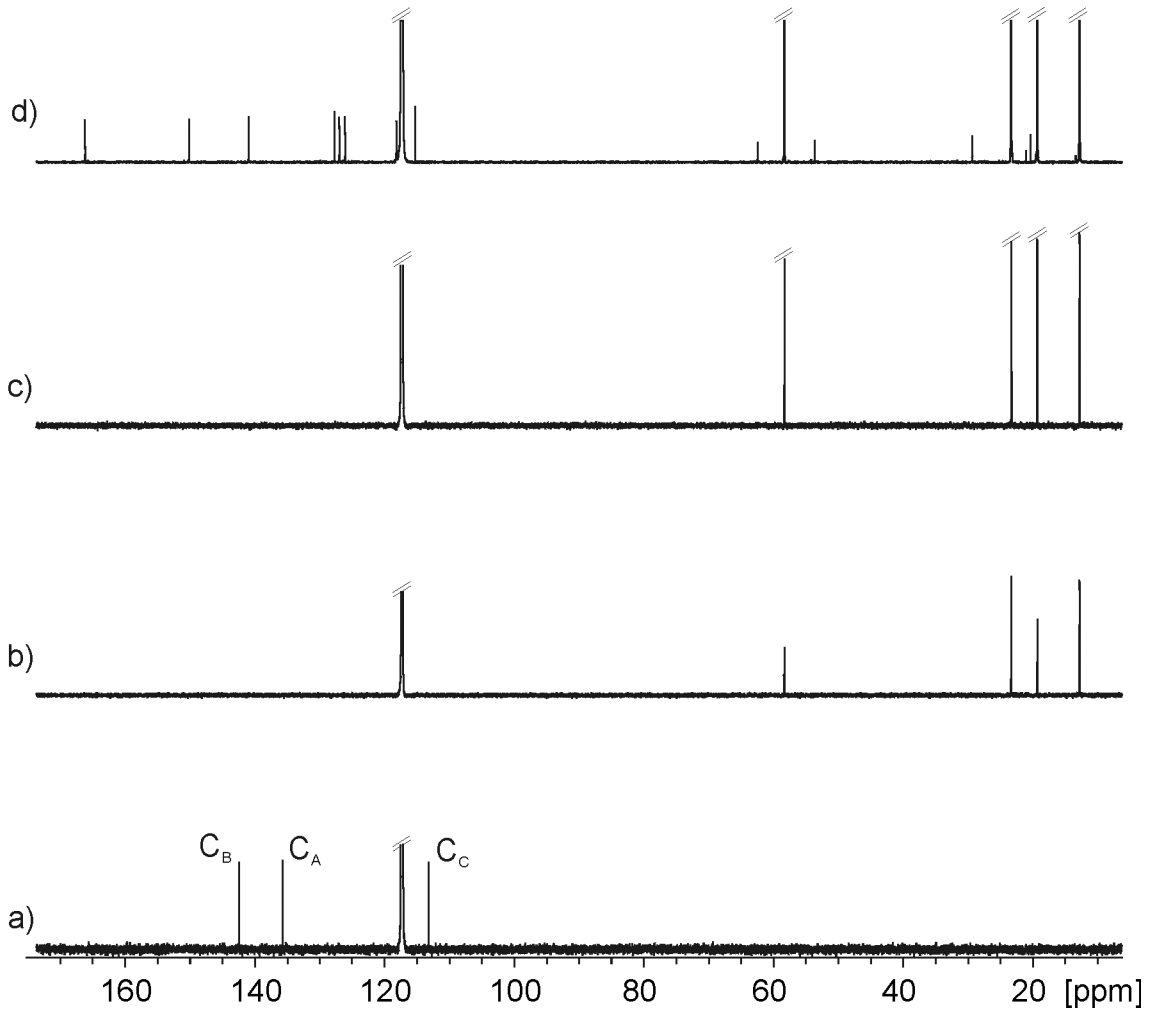

Figure S12. $^{13}C\{^{1}H\}$ NMR spectra (CD_3CN, 298 K) of **[1]** (7 mM) after addition of 0 (a), 1 (b), 3 (c) and 15 equiv (d) of TBAF·$3H_2O$ (512 scans).

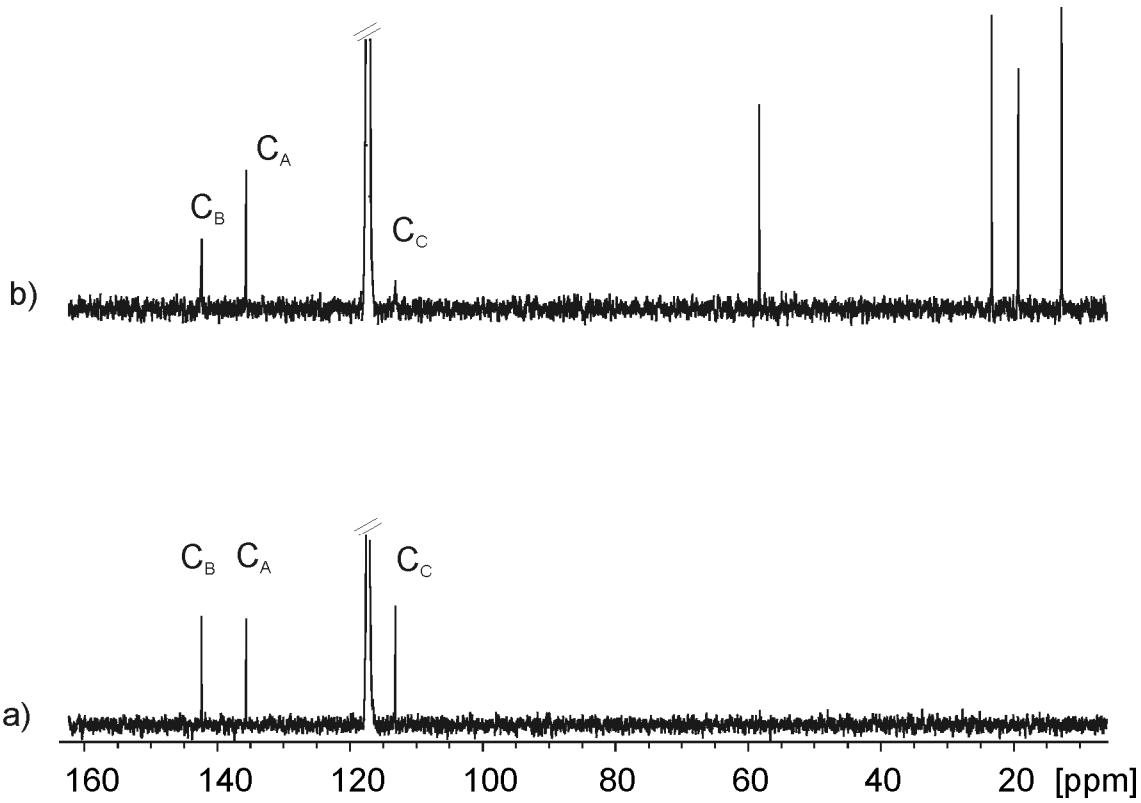

Figure S13. $^{13}C\{^1H\}$ NMR spectra (CD_3CN, 298 K) of **[1]** (7 mM) after addition of: 0 (a), and 1 equivalent of TBAI (b).

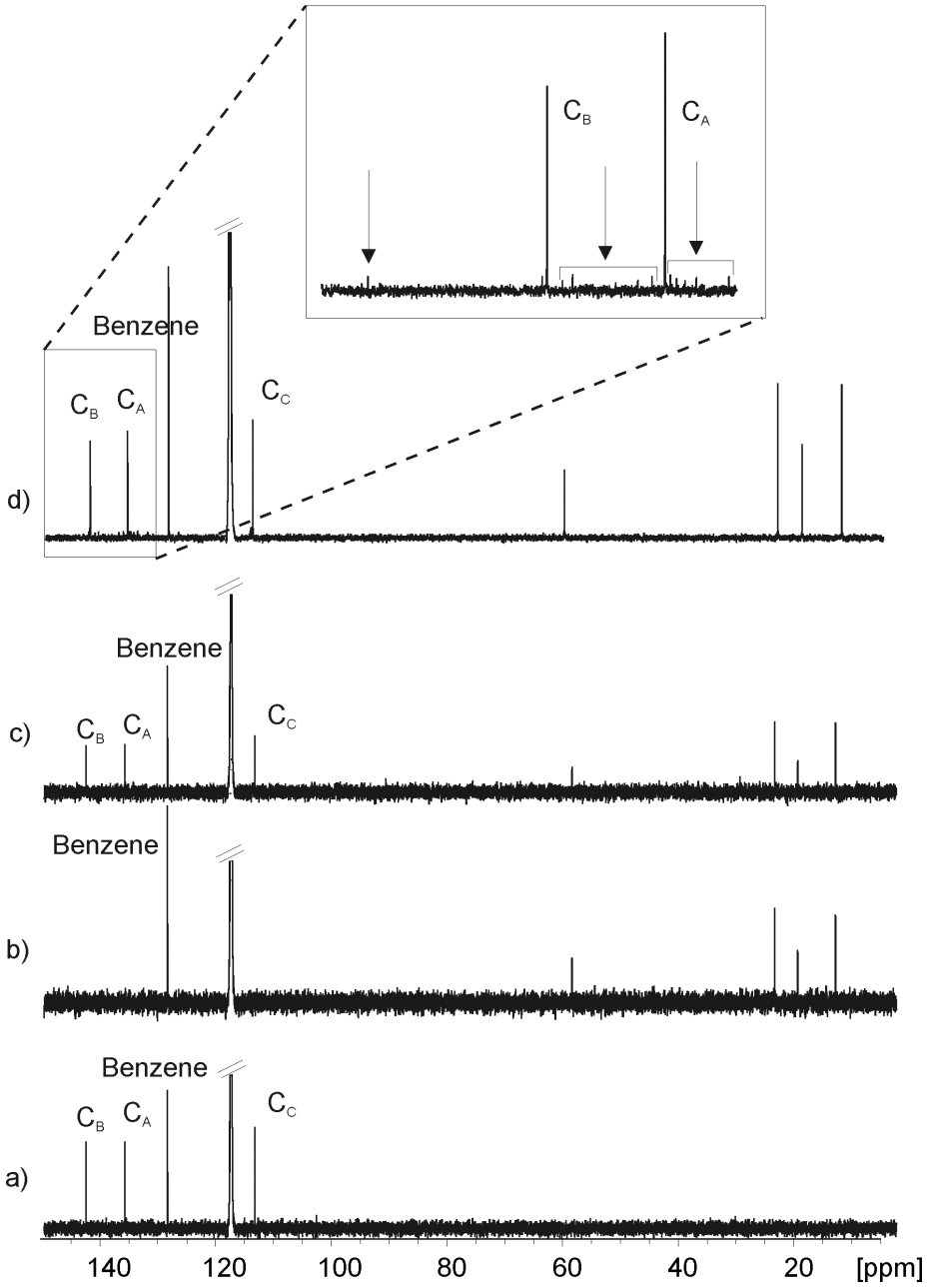

Figure S14. $^{13}C\{^1H\}$ NMR spectra (CD_3CN, 298 K) of **[1]** (7 mM) before (a) and after addition of 1 equivalent of TBAF (b). Addition of 1 equivalent of $NOBF_4$ lead to the oxidation of $[1]^{\bullet-}$ regenerating neutral $HAT(CN)_6$ (c). Spectrum of the solution in (c) with an increased acquisition time (2048 scans) in order to observe the carbon signal of the putative products deriving of the modification of the covalent structure of **1** (d). The covalent modification of the structure of **1** was inferred from the regeneration experiment being non quantitative. Benzene has been used as internal reference to quantify the percentage of regeneration of **1** (~80%). Inset: Expansion of the region from 150 to 130 ppm of spectra (d).

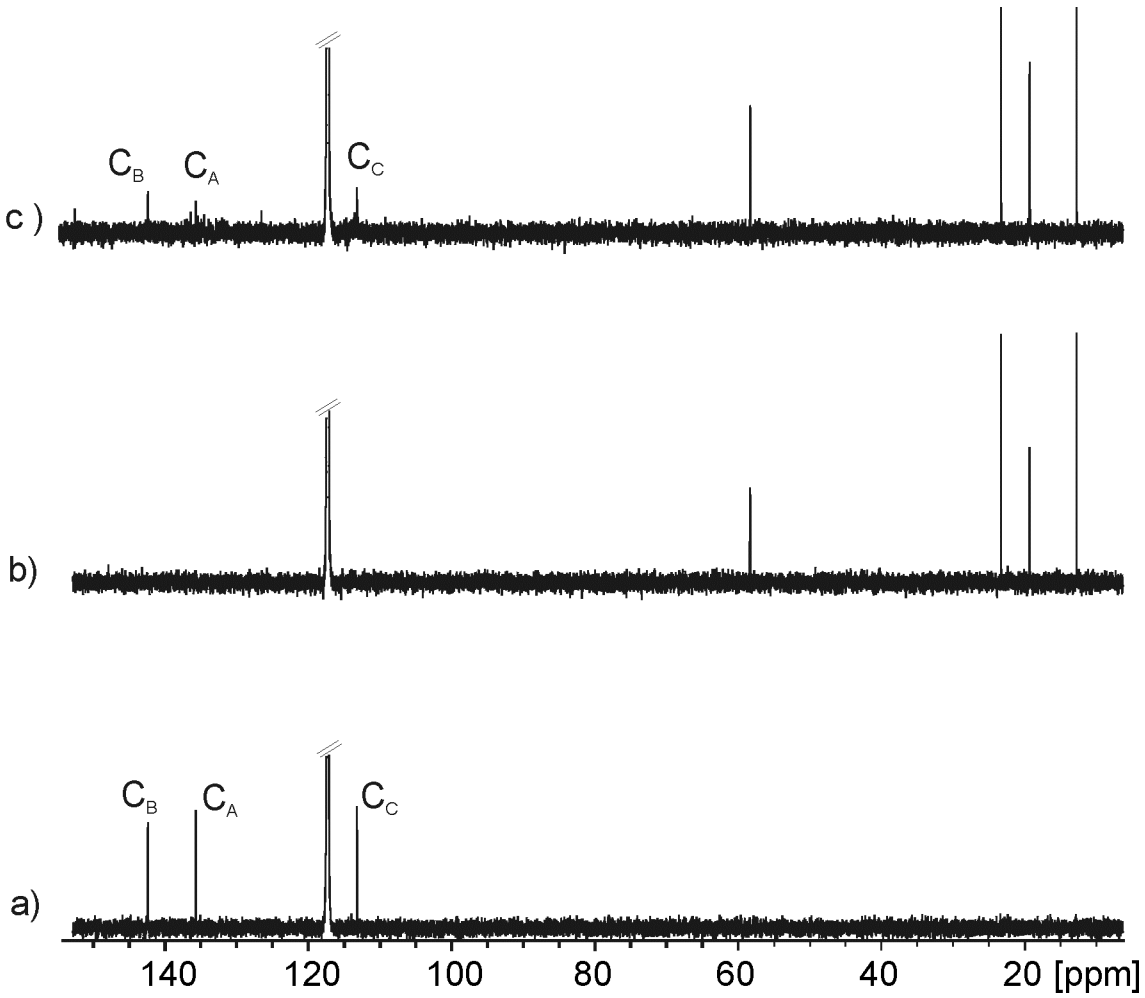

Figure S15. $^{13}C\{^{1}H\}$ NMR spectra (CD_3CN, 298 K) of **[1]** (7 mM) : (a) before (b) after 2 equivalent of TBAF are added and (c) following the addition of more than 3 equivalents of $NOBF_4$ to the previous solution. The oxidation does not produce quantitatively the neutral $HAT(CN)_6$. Subproducts are formed in a significant extent compared to the reoxidized HAT.

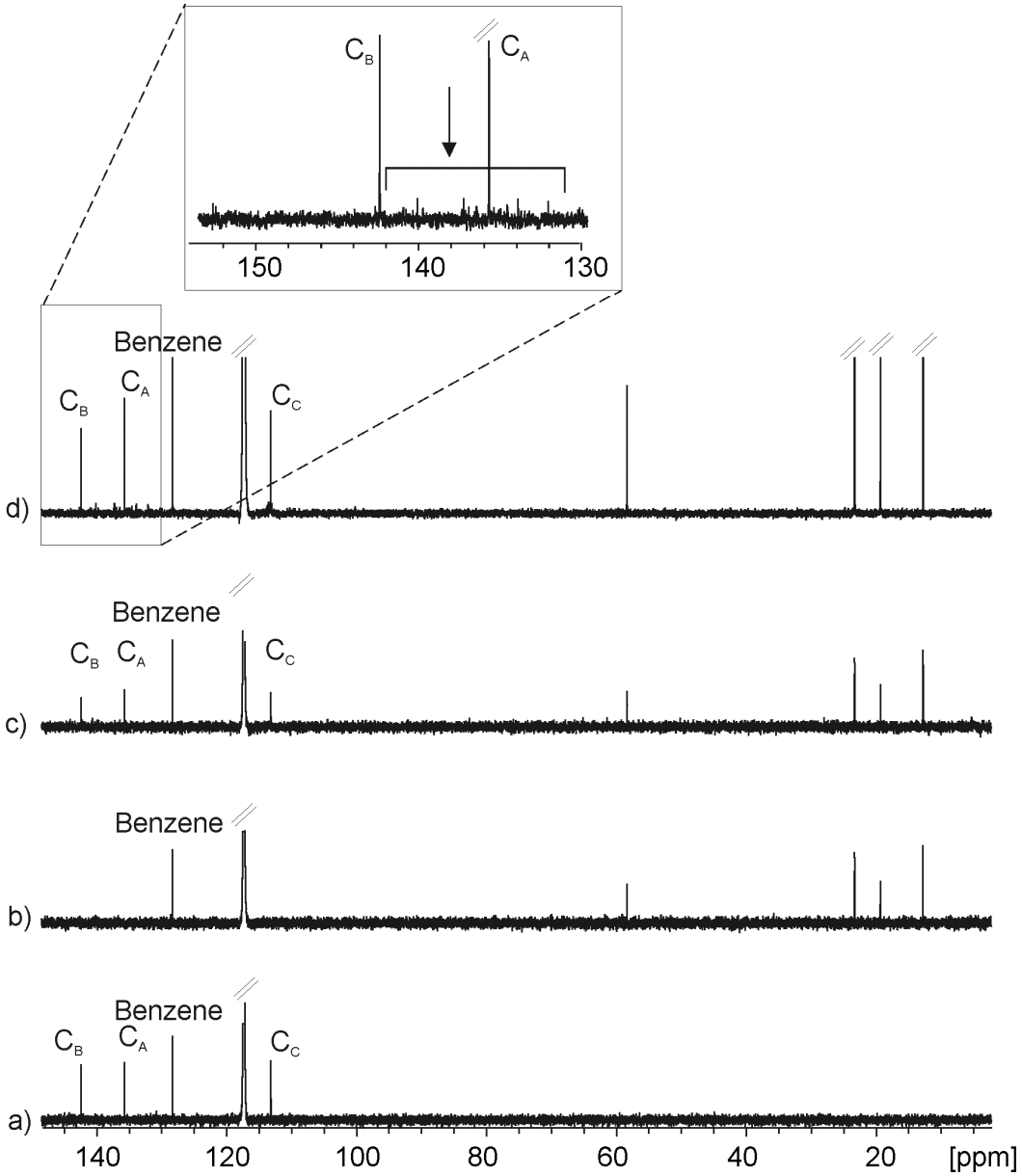

Figure S16. $^{13}C\{^{1}H\}$ NMR spectra (CD_3CN, 298 K) of **[1]** (7 mM): (a) before , (b) after 1 equivalent of TBAOH is added and (c) following the addition of 1 equivalent of $NOBF_4$ to the previous solution. Spectrum of the solution in (c) with an increased acquisition time (2048 scans) in order to observe the carbon signal of the putative products deriving of the modification of the covalent structure of **1** (d). The covalent modification of the structure of **1** was inferred from the regeneration experiment being non quantitative. Benzene has been used as internal reference to quantify the percentage of regeneration of **1** (~40%). Inset: Expansion of the region from 150 to 130 ppm of spectra (d).

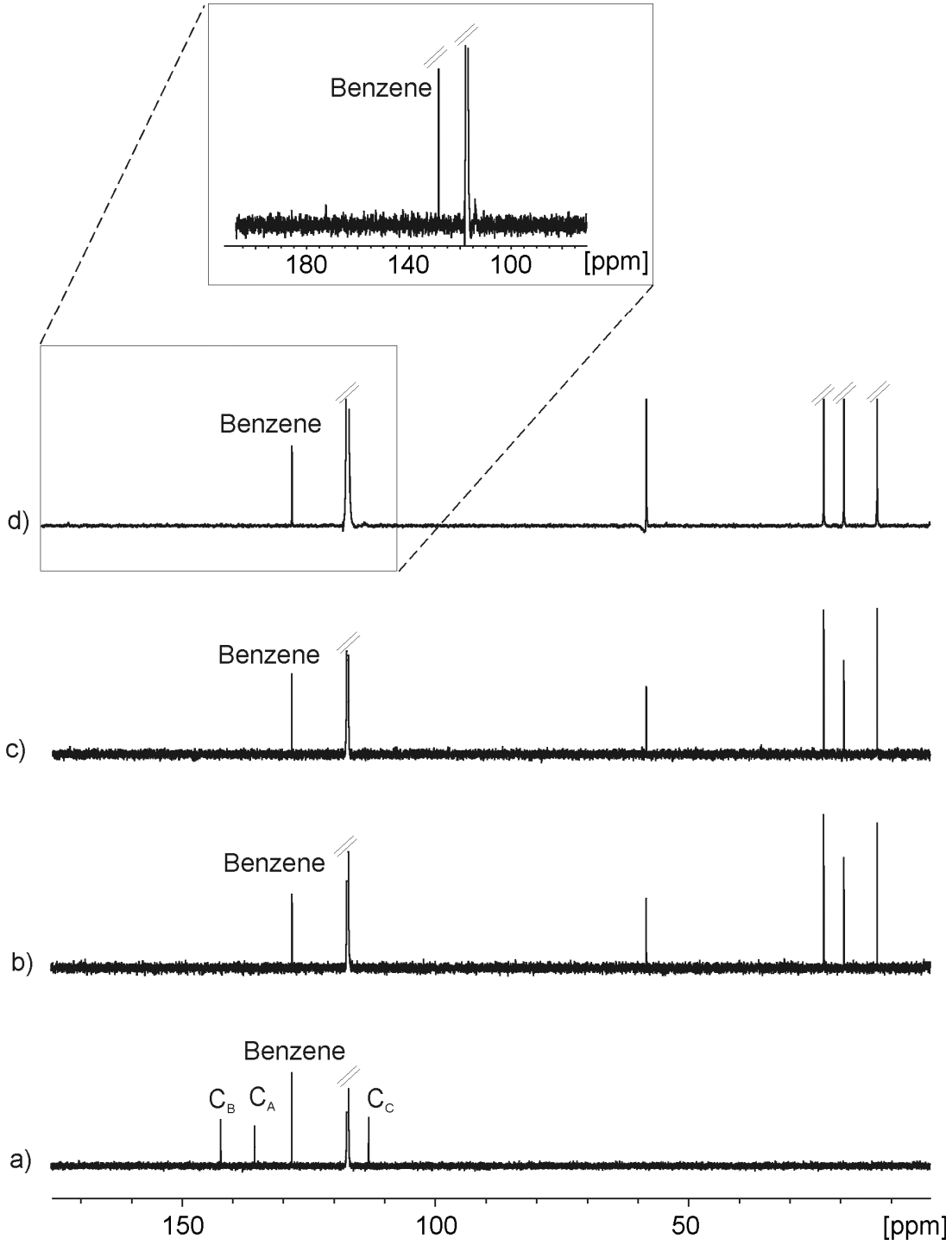

Figure S17. $^{13}C\{^{1}H\}$ NMR spectra (CD_3CN, 298 K) of **[1]** (7 mM): (a) before, (b) after 2 equivalent of TBAOH are added, and (c) following the addition of 5 equivalent of $NOBF_4$ to the previous solution. Spectrum of the solution in (c) with an increased acquisition time (2048 scans) in order to observe the carbon signal of the putative products deriving of the modification of the covalent structure of **1** (d). Inset: Expansion of the region from 200 to 80 ppm of spectra (d).

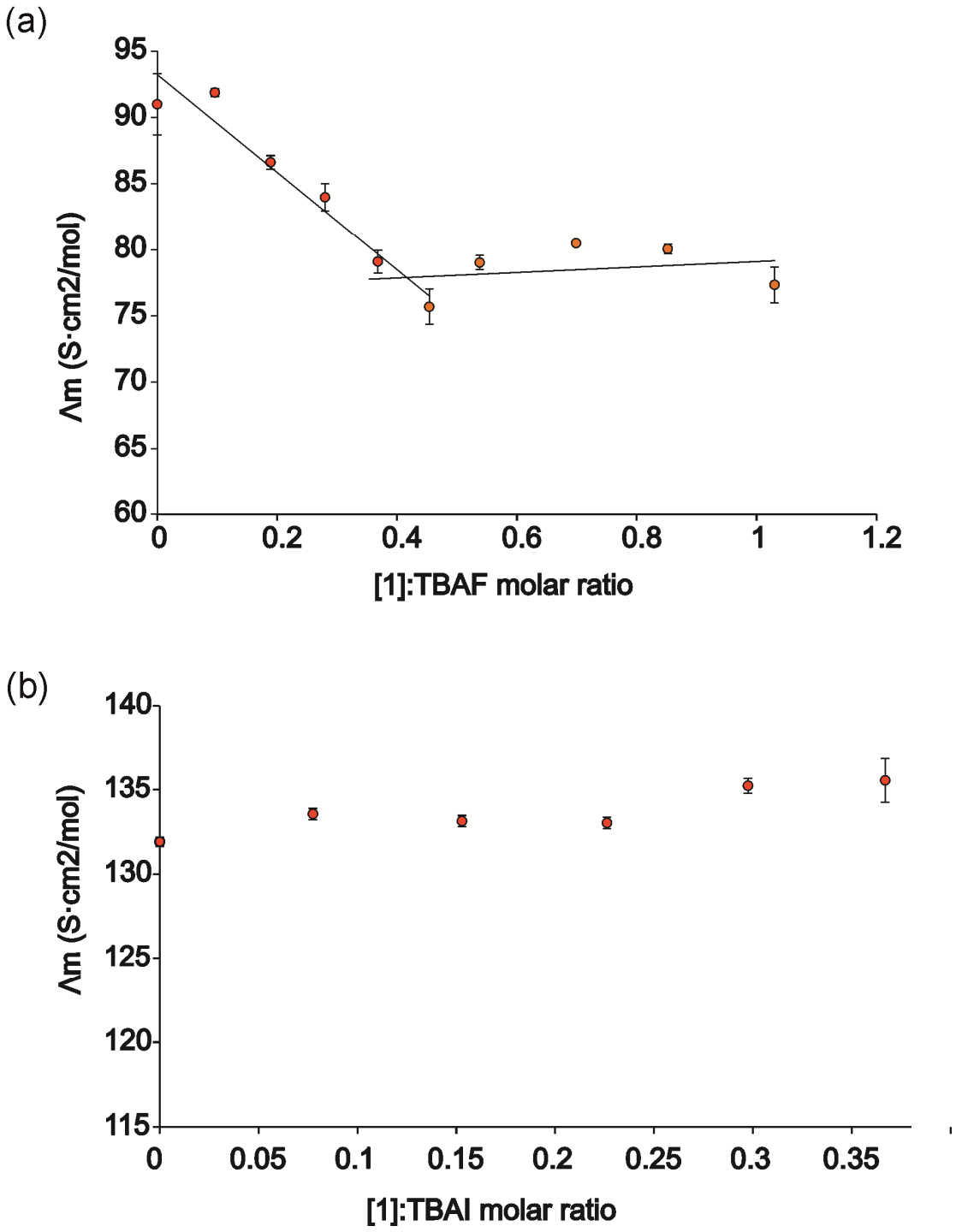

Figure S18. Correlation between conductometric values obtained upon **1**:TBAX molar ratio (X = F (a), I(b)).

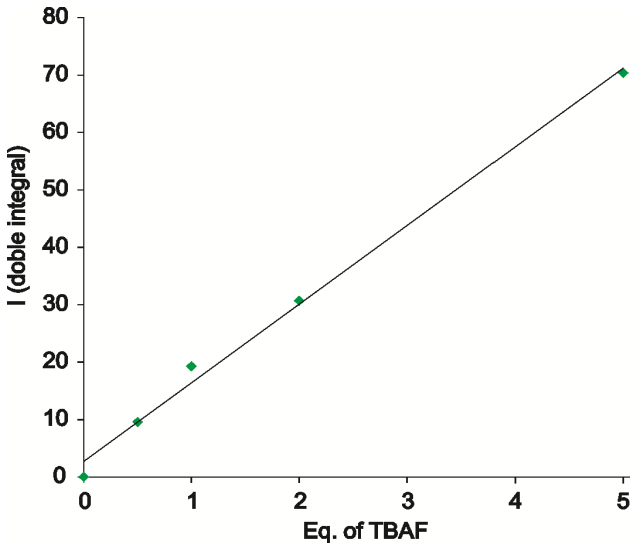

Figure S19. Plot of the linear relationship that exists between the integral of the EPR signal and the concentration of TBAF in the titration experiment of **1**.

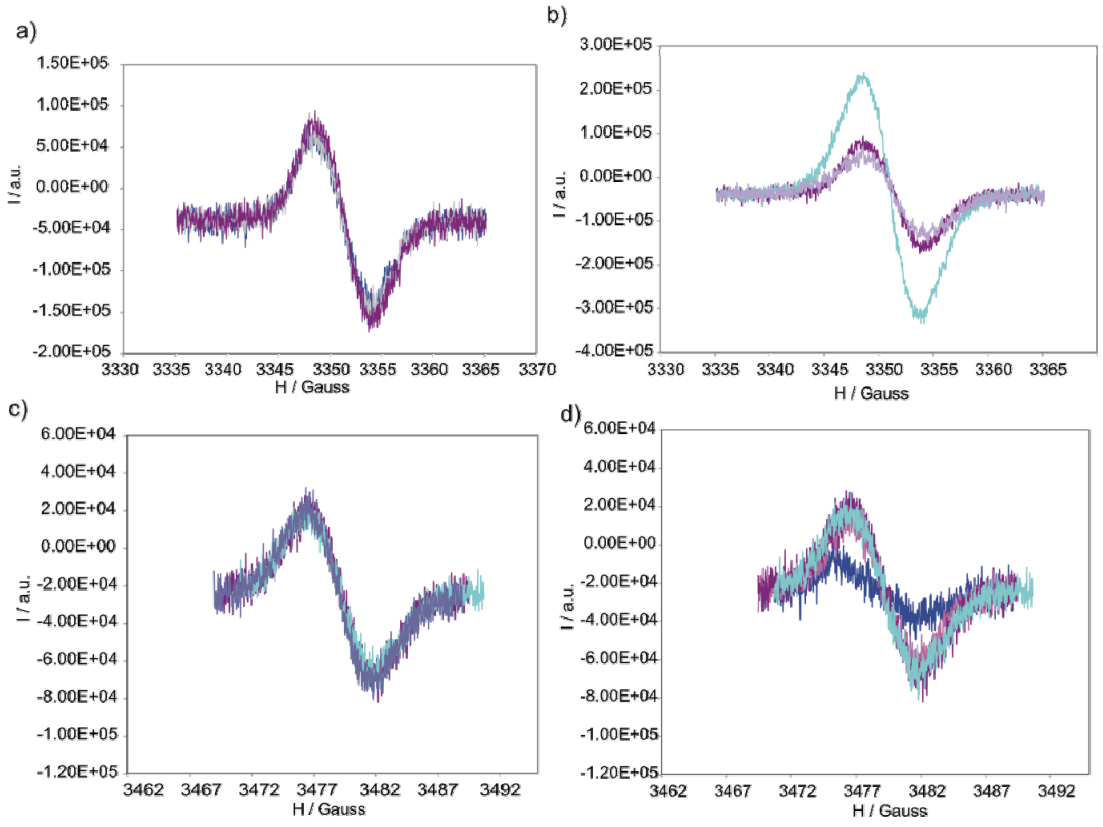

Figure S20. EPR titrations of **1** (0.95 mM) with TBACl (a) and TBABr (c) and photoinduced electron transfer study by EPR titrations of **1** (0.9 mM) with TBACl (b) and TBABr (d).

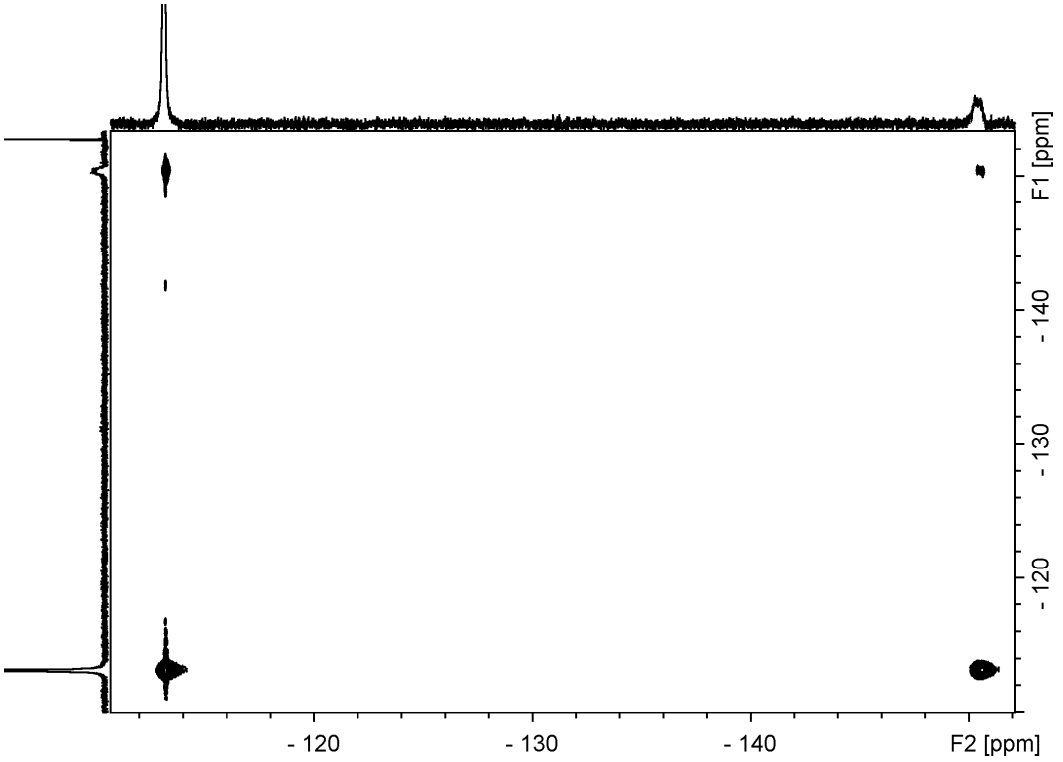

Figure S21. ^{19}F- ^{19}F EXSY NMR experiment at 298 K for a solution of TBAF 31 mM in CH_3CN.

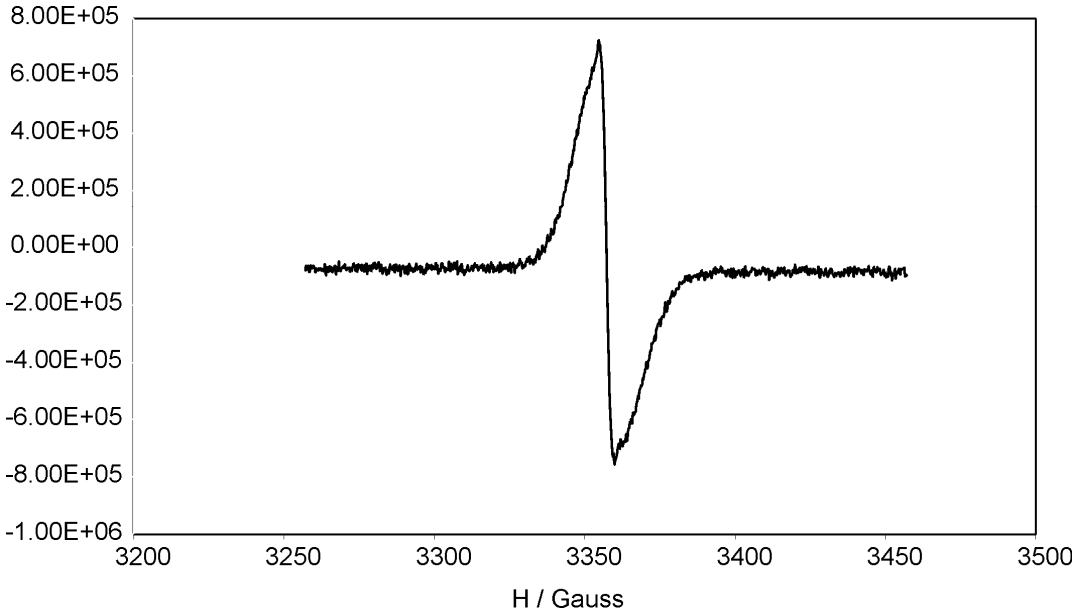

Figure S22. EPR spectrum of a frozen mixture of **1** and 10 equivalent of TBAF at 140 K in CH_3CN.

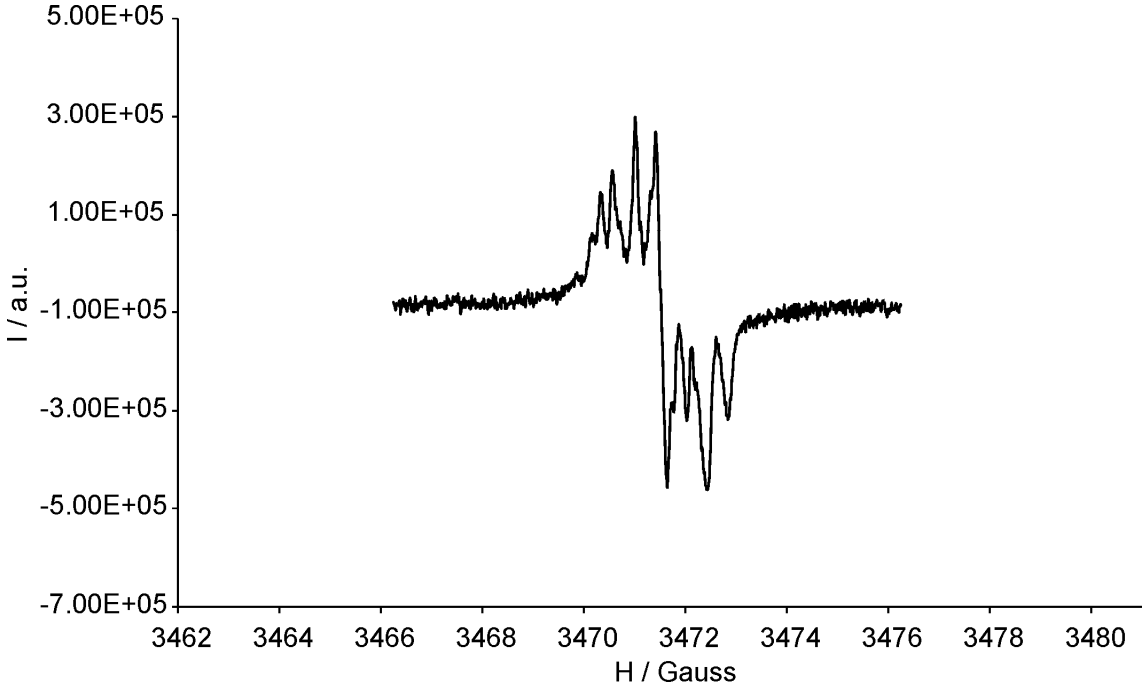

Figure S23. EPR spectrum at 298 K of a CH_3CN solution of **1** containing 2 equivalent of TBAOH.

References

[1] Kanakarajan, K.; Czarnik, A. W. *J. Org. Chem.* **1986**, *51*, 5241.

[2] Shao, S.; Wang, A.; Yang, M.; Jiang, S.; Yu, X. *Synth. Commun.* **2001**, *31*, 1421.

[3] Gaussian 09, Revision B.01, Frisch, M. J.; Trucks, G. W.; Schlegel, H. B.; Scuseria, G. E.; Robb, M. A.; Cheeseman, J. R.; Scalmani, G.; Barone, V.; Mennucci, B.; Petersson, G. A.; Nakatsuji, H.; Caricato, M.; Li, X.; Hratchian, H. P.; Izmaylov, A. F.; Bloino, J.; Zheng, G.; Sonnenberg, J. L.; Hada, M.; Ehara, M.; Toyota, K.; Fukuda, R.; Hasegawa, J.; Ishida, M.; Nakajima, T.; Honda, Y.; Kitao, O.; Nakai, H.; Vreven, T.; Montgomery, Jr., J. A.; Peralta, J. E.; Ogliaro, F.; Bearpark, M.; Heyd, J. J.; Brothers, E.; Kudin, K. N.; Staroverov, V. N.; Kobayashi, R.; Normand, J.; Raghavachari, K.; Rendell, A.; Burant, J. C.; Iyengar, S. S.; Tomasi, J.; Cossi, M.; Rega, N.; Millam, J. M.; Klene, M.; Knox, J. E.; Cross, J. B.; Bakken, V.; Adamo, C.; Jaramillo, J.; Gomperts, R.; Stratmann, R. E.; Yazyev, O.; Austin, A. J.; Cammi, R.; Pomelli, C.; Ochterski, J. W.; Martin, R. L.; Morokuma, K.; Zakrzewski, V. G.; Voth, G. A.; Salvador, P.; Dannenberg, J. J.; Dapprich, S.; Daniels, A. D.; Farkas, Ö.; Foresman, J. B.; Ortiz, J. V.; Cioslowski, J.; Fox, D. J. Gaussian, Inc., Wallingford CT, 2009.

[4] Ahlrichs, R.; Bär, M.; Hacer, M.; Horn, H.; Kömel, C. *Chem. Phys. Lett.*, **1989**, *162*, 165–169.

[5] Tomasi, J.; Mennucci, B.; Cammi, R. *Chem. Rev.*, **2005**, *105*, 2999-3093.